Radiative Heating About Outer Planet Entry Probes

Kenneth Sutton*
NASA Langley Research Center, Hampton, Va.

A study has been conducted to define the radiative, heating-rate distributions about spherically capped, 60° half-angle conical entry probes to the outer planets Jupiter, Saturn, and Uranus. The radiative heating rates are calculated by a direct method for the solution of the inviscid-flow equations with coupled, nongray radiative transport. Results are presented for a range of entry conditions using atmospheric models denoted as nominal, warm, and cool for each planet, and show that both the magnitude and distribution of radiative heating rate are strongly dependent on the atmospheric model and the freestream conditions.

Nomenclature

A_b = probe base area, m^2
A_ρ = atmospheric pre-exponential parameter [Eq. (1)], kg/m^3
B_ρ = atmospheric exponential parameter [Eq. (1)], m^{-1}
C_d = drag coefficient
c_i = mass fraction of element i
K = convective heat-transfer coefficient [Eq. (8)], $kg^{1/2}/m$
M = Mach number
m = probe mass, kg
p = pressure, atm (1 atm = $1.01 \times 10^5 N/m^2$)
q^C = cold-wall convective heating rate, W/m^2
q^R = radiative heating rate, W/m^2
R_n = body nose radius, m
r_b = body base radius, m
s = distance along body surface, m
T = temperature, K
$\bar{t}, t$ = entry time from 500 km [Eqs. (3) and (5)], sec
V = velocity, m/s
y = distance normal to body surface, m
Z = altitude, m
α = entry angle, deg
$\bar{\beta}, \beta$ = ballistic coefficient [Eq. (4)], kg/m^2
δ = local shock stand-off distance normal to body surface, m
ϵ = density ratio across normal shock
θ_c = cone half angle, deg
θ_δ = local shock angle, deg
ρ = density, kg/m^2

Subscripts

E = entry
0 = stagnation point
s = normal shock
w = wall
∞ = freestream

Introduction

EXPLORATORY missions to the outer planets of Jupiter, Saturn, and Uranus by instrumented entry probes are currently being considered for 1979-1984 to obtain measurements that will increase our understanding of these planets and their atmospheres. The probes will experience a severe aerothermodynamic environment with high levels of both convective and radiative heating. Accurate predictions of the heating rates are necessary to design minimum weight heat shields which insure survival of the probes, since it is estimated that 25-50% of the probes' weight will be heat shield.

Radiative heating can be a dominant mode of heat transfer to the probes for the outer planet entries. Previous studies for entries in the Earth and Venusian atmospheres have shown that radiative heating rates to downstream regions of probes can exceed, under certain conditions, the stagnation region values.[1-4] Since most of the heat-shield surface and weight are in the downstream region of a probe, reliable predictions of the radiative heating rates are needed there as well as in the stagnation region. Earlier studies[5,6] of the radiative heating rates for outer planet probes employed approximate techniques that attempted to extrapolate or extend stagnation region results to the downstream region. A recent study[7-8] for Saturn and Uranus entries obtained results for the downstream region by specifying the shock shape by an approximate method. Since radiative transport depends upon the thickness of the shock layer and the distribution of temperature and density across the shock layer, inaccuracies in these quantities could lead to erroneous radiative heating rates and distribution of the rates along the probe surface.

This study was undertaken to insure a greater degree of confidence in the prediction of radiative heating rates about probes during outer planet entry by considering the solution of the radiative inviscid flow and shock shape in greater detail than prior studies. A range of entry conditions and atmospheric models which are currently under consideration for entries to Jupiter, Saturn, and Uranus by a spherically capped, 60-deg half-angle conical body are investigated.

Solution Procedure

The results of the present study are based on a solution of the equations for the inviscid, radiative flow about an axisymmetric blunt body by a second-order, time-asymptotic numerical method. The divergence of the radiative flux is included in the energy equation to account for nongray radiative transport with continuum and atomic line transition. The solution is a direct method in that the shock shape and internal flowfield parameters are solved for a specified body shape. The basic form of the present method has been used in prior studies for the inviscid, radiative flow about planetary entry bodies and also as an integral part of a fully coupled method with a boundary-layer solution, including ablation product injection, for Venusian entries.[1-3] In this study the basic inviscid method[1] was modified to account for attachment of the sonic line to the wall at the aft corner of a body by the method presented in Refs. 9 and 10.

The solutions to the radiative, inviscid flow about the probe are obtained at selected times during an entry. An Allen-

Presented as Paper 75-183 at the AIAA 13th Aerospace Sciences Meeting, Pasadena, Calif., Jan. 20-22, 1975; submitted Jan. 28, 1975; revision received December 1, 1975.

Index categories: Radiatively Coupled Flows and Heat Transfer; Entry Vehicles and Landers.

*Head, Entry Heating Analysis Group, Aerothermodynamics Branch, Space Systems Division. Member AIAA.

Eggers type of analysis for an exponential atmosphere is used to define a trajectory[11]

$$\rho_\infty = A_\rho \exp(-B_\rho Z) \tag{1}$$

$$V_\infty = V_E \exp(-\rho_\infty / 2A_\rho \bar{\beta}) \tag{2}$$

$$\bar{t} = \int_Z^{Z_E} \frac{1}{V_\infty} dZ \tag{3}$$

Modified forms of the ballistic coefficient and entry time defined as

$$\bar{\beta} = -\beta \sin \alpha_E \tag{4}$$

$$\bar{t} = -t \sin \alpha_E \tag{5}$$

where

$$\beta = m/C_d A_b \tag{6}$$

are used so that a calculated trajectory can refer to a combination of ballistic coefficients and entry angles. Variation in the ballistic coefficient during an entry due to mass loss and probe shape change from ablation of the heat shield is not considered.

The wall pressures, cold-wall convective heating rates, and radiative heating rates to the stagnation point of a hemisphere are also calculated. The wall pressures are given by

$$P_{w,0} \approx 9.4 \times 10^{-6} \rho_\infty V_\infty^2 \tag{7}$$

The cold-wall convective heating rates are approximated by

$$q^c_{w,0} \sqrt{R_n} \approx 0.487 K \rho_\infty^{1/2} V_\infty^3 \tag{8}$$

$$K = 2.50 \times 10^{-4} (4.07 c_H + c_{He})^{1/2} \tag{9}$$

which is based on data presented in Ref. 12. The radiative heating rates are obtained from a matrix of solutions generated by a stagnation-point solution of the previously described method for a radiative, inviscid flowfield.

III. Entry Parameters and Gas Composition

The present study considered entry to Jupiter, Saturn, and Uranus at a fixed entry velocity for each planet with a range of entry angles and ballistic coefficients as listed in Table 1. The entry conditions are relative to the particular planet and time is measured from an altitude of 500 km [Z_E in Eq. (3)]. The probe is a spherically capped, conical body with a nose radius of 22.3 cm, a half angle of 60 deg and a base-to-nose-radius ratio of 2. A schematic of the body shape and coordinate system is shown in Fig. 1.

The exact structure of the outer planet atmospheres is unknown, and thus it is necessary to account for the possibility of different atmospheres in a heating analysis. The atmospheric models denoted as nominal, warm, and cool,[13-15] in which the dominant species are helium and diatomic hydrogen, are used in the present study. Listed in Tables 2 and 3 are the constants which describe the density profiles, [Eq. (1)] and the elemental mass fractions of the gas composition. The density constants were selected to match the density profiles[13-15] in the density range of 10^{-3}-10^{-5} kg/m^3, where radiative heating occurs during an entry. Zero altitude is set at a pressure of 1 atm (1.01×10^5 N/m^2) for Jupiter and Saturn and at the correspondence level for Uranus.[13-15] The elemental mass fractions are slightly different from those given in Refs. 13-15 in that trace species are neglected and slight adjustments are made so that the nominal and warm atmospheres have the same mass fraction of hydrogen for all three planets and the cool atmosphere has the same mass fraction of hydrogen for Jupiter and Saturn. These adjustments of the mass fractions are less than 10% and should not appreciably affect the results to be presented. The radiation from helium is neglected because experimental results have shown that, even for a helium-enriched mixture, helium contributes less than 1% of the total radiation for a hydrogen-helium mixture.[16,17]

Table 1 Entry parameters

Planet	V_E, km/s	α_E, deg	β, kg/m^2	$\bar{\beta}$, kg/m^2
Jupiter	47.5	-10 to -15	121 to 149	21.0 to 38.6
Saturn	32.0	-20 to -50	121 to 149	41.4 to 114.1
Uranus	26.0	-25 to -50	121 to 149	51.1 to 114.1

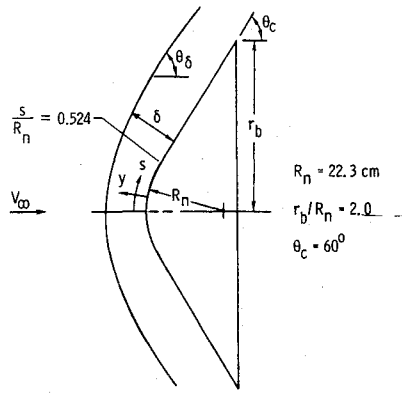

Fig. 1 Body shape and coordinate system.

Table 2 Atmospheric parameters

Planet	Atmos.	A_ρ, kg/m^3	B_ρ, m^{-1}
Jupiter	Warm	0.102	3.69×10^{-5}
	Nominal	.119	4.77×10^{-5}
	Cool	.308	8.11×10^{-5}
Saturn	Warm	.750	2.42×10^{-5}
	Nominal	.711	3.68×10^{-5}
	Cool	.655	5.55×10^{-5}
Uranus	Warm	.071	2.23×10^{-5}
	Nominal	.487	3.67×10^{-5}
	Cool	5.221	8.11×10^{-5}

Table 3 Elemental mass fractions

Planet	Atmosphere	c_H	c_{He}
Jupiter, Saturn, Uranus	Warm	0.90	0.10
Jupiter, Saturn, Uranus	Nominal	.79	.21
Jupiter, Saturn	Cool	.55	.45
Uranus	Cool	.20	.80

IV. Results and Discussion

The calculated entry trajectories for the nominal atmospheres are shown in Fig. 2. Using the nominal atmosphere

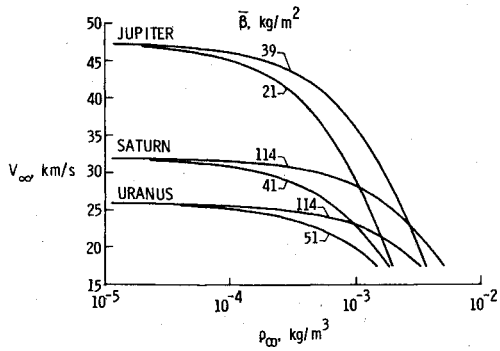

Fig. 2 Entry trajectories for nominal atmospheres.

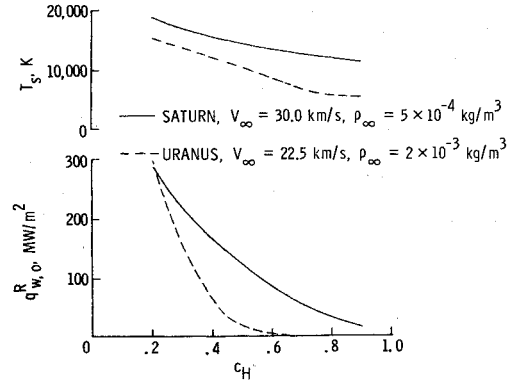

Fig. 3 Effects of gas composition.

case as a reference, there is a deeper penetration of the probe at high velocities into the denser regions of a cool atmosphere and less penetration in a warm atmosphere. Listed in Table 4 are the maximum values along a trajectory of the wall pressure, cold-wall convective heating rate and the radiative heating rate at the stagnation point of a hemisphere. These maximum values vary almost linearly with respect to ballistic coefficient between the limits listed. The most severe environment is for entry into a cool atmosphere. Note that the radiative heating rate can range from values which are negligible relative to the convective heating for entries in a warm or nominal atmosphere of Uranus to an extremely high value of 1670 MW/m^2 for an entry in a cool atmosphere of Jupiter.

One of the primary causes for the larger values of heating rates and pressure for entries in a cool atmosphere is the deeper penetration. A second cause if the effect of a gas composition; a cool atmosphere has a larger amount of helium. Temperatures in the flowfield increase with increased amounts of helium because oflium has fewer internal degrees of freedom to accommodate the energy than does hydrogen.[7] The dependence of cold-wall convective heating rate on gas composition can be seen from examination of Eq. (9). The effect of gas composition on stagnation-point, radiative heating rate is shown in Fig. 3 at freestream conditions typical of entry to Saturn and Uranus. Radiative heating is strongly dependent on temperature; and, as shown by the data, the temperature and radiative heating rate increase for entry into both planets as the mass fraction of hydrogen is reduced.

Solutions to the radiative, inviscid flow about a probe were obtained at selected points along the trajectories for the conditions listed in Table 5. In general, the distribution of radiative heating rates is influenced by decreasing pressure and temperature and increasing shock-layer thickness as the gas expands around the body. These effects can influence line and continuum radiation in different ways.

The stagnation-point radiative heating pulse for entry in a Jupiter nominal atmosphere is shown in Fig. 4. At the times indicated by the circular symbols, the distributions of radiative heating rates along the body were calculated, and the results are shown in Fig. 5. The radiative heating rates decrease from the stagnation-point value along the forward region of the body to a minimum in the vicinity of the tangency point and then increase along the conical region to values which can be greater than the stagnation-point value. The distributions are nonsimilar during the entry, being strongly dependent on freestream conditions. The larger heating rates over the body, relative to the stagnation-point value, occur

Table 4 Maximum values during entry

Planet	Atmos.	$\bar{\beta}$, kg/m^2	$q^R_{w,o}$ MW/m^2	$q^C_{w,o}$ MW/m^2	$p_{w,o}$ atm
Jupiter	Warm	21.0	157	139	6.0
		38.6	365	188	11.0
	Nominal	21.0	274	165	7.8
		38.6	622	224	14.3
	Cool	21.0	823	244	13.3
		38.6	1672	330	24.3
Saturn	Warm	41.4	3	48	3.4
		114.1	10	80	9.8
	Nominal	41.4	11	63	5.4
		114.1	42	104	14.8
	Cool	41.4	70	87	8.1
		114.1	284	144	22.4
Uranus	Warm	51.1	0.01	28	2.7
		114.1	.04	41	5.9
	Nominal	51.1	.07	37	4.4
		114.1	.25	56	9.8
	Cool	51.1	153	80	9.7
		114.1	436	120	21.6

Table 5 Conditions for body solutions

Planet	Atmos.	$\bar{\beta}$, kg/m^2	$\bar{t}$, s	V_∞, km/s	ρ_∞, kg/m^3	ε
Jupiter	Nominal	21.0	7.00	46.83	3.96×10^{-5}	12.93
			7.59	44.22	1.43×10^{-4}	11.72
			8.09	39.09	3.90×10^{-4}	10.43
			8.51	31.90	7.98×10^{-4}	9.06
			8.70	28.19	1.06×10^{-3}	8.73
		31.3	8.21	40.00	5.20×10^{-4}	10.37
		38.6	8.36	39.00	7.25×10^{-4}	10.04
	Warm	21.0	7.29	39.36	2.91×10^{-4}	10.44
		21.0	8.15	27.47	8.27×10^{-4}	9.44
		38.6	7.65	39.22	5.45×10^{-4}	10.05
	Cool	21.0	9.02	36.85	8.65×10^{-4}	10.06
		21.0	9.31	27.63	1.85×10^{-3}	8.36
		38.6	9.02	40.50	1.00×10^{-3}	10.33
Saturn	Nominal	41.4	9.05	29.15	2.83×10^{-4}	9.17
		77.4	8.49	31.13	1.57×10^{-4}	9.67
			9.74	28.70	6.30×10^{-4}	8.88
			10.15	27.07	9.53×10^{-4}	8.89
		114.1	10.20	28.19	1.06×10^{-4}	8.73
	Warm	77.4	5.40	29.92	2.52×10^{-4}	9.30
		114.1	5.90	29.92	3.71×10^{-4}	9.18
		114.1	7.08	27.47	8.47×10^{-4}	9.44
	Cool	41.4	11.80	27.88	6.33×10^{-4}	8.84
		77.4	13.00	21.16	3.82×10^{-3}	9.35
		114.1	12.03	29.50	1.00×10^{-3}	8.90
		114.1	12.41	27.63	1.83×10^{-3}	8.36
Uranus	Nominal	114.1	12.08	24.50	5.00×10^{-4}	10.33
	Cool	51.1	14.67	24.97	3.34×10^{-4}	9.12
			15.53	21.20	1.69×10^{-3}	7.49
			15.88	18.13	2.99×10^{-3}	6.68
		114.1	15.18	24.69	9.60×10^{-3}	8.53
			15.91	21.16	3.82×10^{-3}	7.17
			16.21	18.60	6.21×10^{-3}	6.56
			16.38	16.95	7.90×10^{-3}	6.44

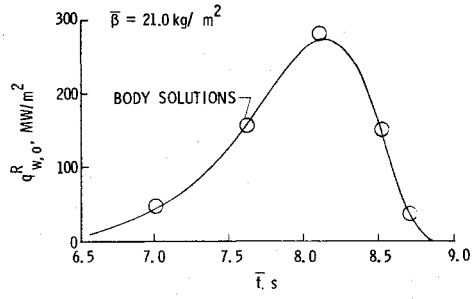

Fig. 4 Radiative heating pulse for Jupiter entry with nominal atmosphere.

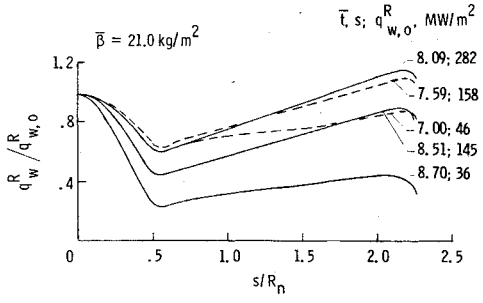

Fig. 5 Radiative heating distributions for Jupiter entry with nominal atmosphere.

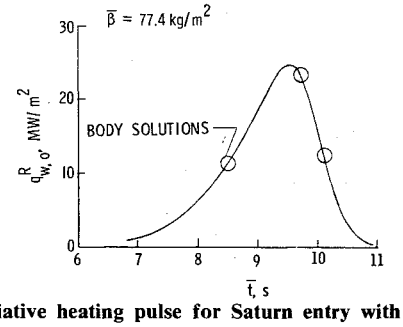

Fig. 6 Radiative heating pulse for Saturn entry with nominal atmosphere.

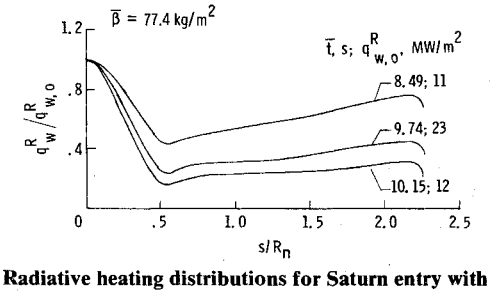

Fig. 7 Radiative heating distributions for Saturn entry with nominal atmosphere.

near the time of peak stagnation-point heating rate. For all of the Jupiter entries studied, the nondimensional radiative heating distributions near the time of peak stagnation-point heating are approximately the same as the distributions shown in Fig. 5 at the times of 7.59. and 8.09.

The radiative heating pulse for entry in a Saturn nominal atmosphere is shown in Fig. 6; and, at the times indicated, the radiative heating distributions are shown in Fig. 7. For this entry, the largest nondimensional value of radiative heating rate along the body occurs at an earlier time, $\bar{t}=8.49$, rather than at the time of peak stagnation-point radiative heating rate ($\bar{t}\approx 9.74$). The heating rates along the flank region will be comparable to the heating rates along the flank at time of

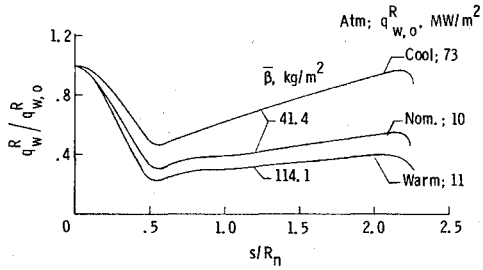

Fig. 8 Effects of atmosphere on radiative heating distributions for Saturn entry at times near peak stagnation-point radiative heating rate.

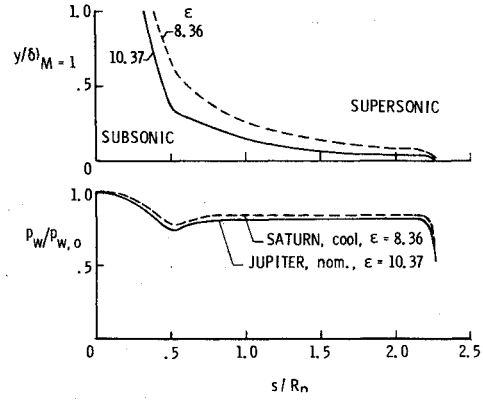

Fig. 9 Examples of sonic line location and pressure distributions for Jupiter and Saturn entries.

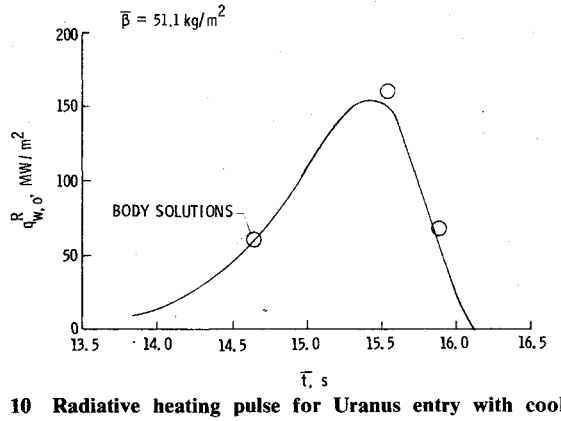

Fig. 10 Radiative heating pulse for Uranus entry with cool atmosphere.

peak stagnation-point heating rate, even though the stagnation-point value at this time is one-half of the peak stagnation-point value.

The distributions at times of peak stagnation-point radiative heating rate for entries into a warm, nominal, and cool atmosphere for Saturn entry are compared in Fig. 8. The nondimensional heating rates along the flank region increase to different values, with the largest values occurring for the cool atmosphere.

Before proceeding to a discussion of the radiative heating distributions for Uranus entries, results that illustrate the type of flow over the probes for Jupiter and Saturn entries are presented in Fig. 9. As shown in the figure, the sonic line is attached to the shock wave at the forward region of the flowfield and approaches the body in an asymptotic manner to attach at the aft corner. Thus, the flow is mixed, being subsonic in the forward region and the region adjacent to the body and supersonic in the flank region adjacent to the shock wave. The wall pressure is constant along the flank and then

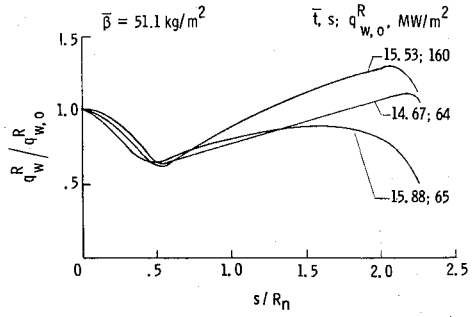

Fig. 11 Radiative heating distributions for Uranus entry with cool atmosphere.

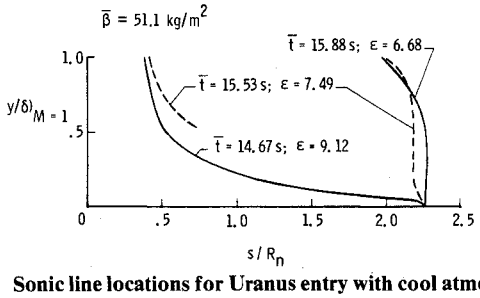

Fig. 12 Sonic line locations for Uranus entry with cool atmosphere.

expands at the corner to sonic conditions. The effects of this expansion are localized to the vicinity of the corner, $2.15 \leq s/R_n \leq 2.25$, and cause the slight decrease in the radiative heating rates at the end of the body. The flow over the forward region of the body, up to the cone tangency point, is the same as over a hemisphere at equivalent freestream conditions. This type of flow occurs for all cases studied for the 60-deg body for Jupiter and Saturn entries. However, for entries in the cool atmosphere of Uranus, the results show a different flow pattern.

The stagnation-point radiative heating pulse for entry with $\bar{\beta} = 51.1$ kg/m^2 into the Uranus cool model atmosphere is shown in Fig. 10; and, for the times indicated, the radiative heating distributions are presented in Fig. 11. As was seen previously for the Jupiter and Saturn entry, the distributions are not similar along the trajectory. Of particular interest in this case is the distribution for $\bar{t} = 15.88$ sec for which the radiative heating reaches a local maximum at a point on the conical surface much farther ahead of the aft shoulder than for the two earlier times. This effect can be explained by the type of flow over the body as characterized by the sonic line locations shown in Fig. 12. At the earliest time, the sonic line location is similar to those previously presented for Jupiter and Saturn. At the intermediate time, near peak heating, the character of the flow is different; transonic flow exists throughout much of the shock layer along the conical flank. Because of the accuracy criterion employed to permit reasonable computational times for the solution, it was not possible to accurately locate the sonic line through the flow for which the local Mach number varies only a few percent from one. Only those portions of the sonic line that could be easily defined are shown. For this case, the influence of the corner on the radiative heating distribution seems to extend farther upstream than for the case at the earliest time. Finally, at the latest time, the sonic line is located near the end, or corner, of the body and the flow over the entire body is subsonic. As a result, the influence of the corner is felt well upstream of the corner. The drastic shift in sonic line location as the trajectory is traversed is a result of a decrease in normal shock density ratio from 9.12 to 6.68. The same behavior also occurs for entry into the Uranus cool model atmosphere with $\bar{\beta} = 114.1$ kg/m^2.

Values of density ratio across a normal shock are listed in Table 5 for the cases considered in this study. The following

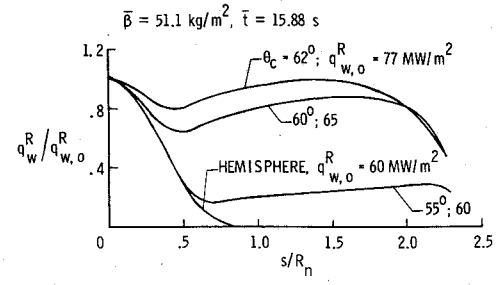

Fig. 13 Effect of body shape on radiative heating distributions for Uranus entry with cool atmosphere.

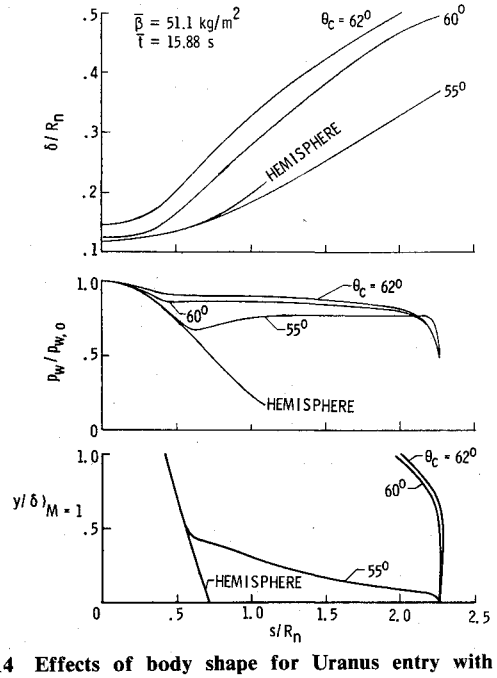

Fig. 14 Effects of body shape for Uranus entry with cool atmosphere.

trends are noted for the spherically capped, 60-deg half-angle conical body. The flow will be mixed, with subsonic flow in the forward region and adjacent to the body and supersonic flow in the region adjacent to the shock wave along the cone flank for density ratios greater than approximately 8.3. At density ratios less than approximately 7.0, the flow will be subsonic over the entire body. Between density ratios of approximately 7.0 and 8.3, especially in the range of 7.15 to 7.50, the flow will be transonic in the flank region.

Small oscillations in angle of attack might also result in significant shifts in sonic line location. To explore this possibility, radiative heating distributions for a hemisphere and spherically capped, conical bodies of $\theta_c = 55$,60, and 62 deg were computed for the Uranus cool atmosphere shallow trajectory, at freestream conditions for $\bar{t} = 15.88$ sec on the radiative heating pulse shown in Fig. 10. The results are presented in Fig. 13. While small changes in cone half-angle do not directly equate to small variations in angle of attack about zero, the results for the 62-deg half-angle cone can be taken as a first approximation to the flow along the windward ray of a 60-deg half-angle cone at an angle of attack of 2-deg. Likewise, the results for the 55-deg half-angle cone can represent a first approximation to the flow along the leeward ray of a 60-deg body at 5-deg angle of attack. The most obvious effect of a relatively small change in angle of attack is a variation in the local heating rate maximum on the conical surface of from 18 to 76 MW/m^2. A change in stagnation-

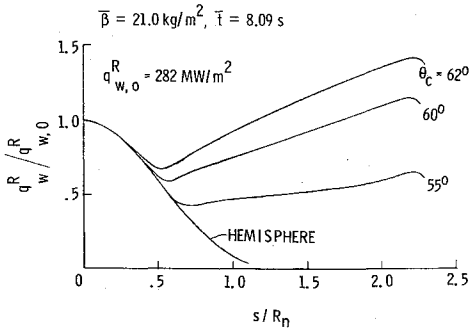

Fig. 15 Effect of body shape on radiative heating distributions for Jupiter entry with nominal atmosphere.

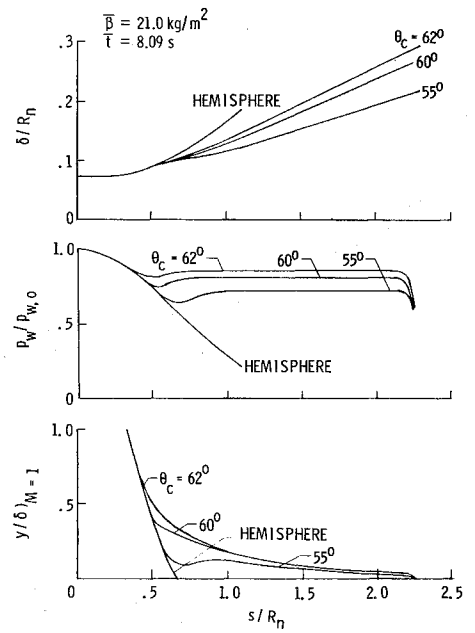

Fig. 16 Effects of body shape for Jupiter entry.

point heating between 60 and 77 MW/m^2 is also noted. Finally, from the good agreement between the results for the 55-deg half-angle body forward of the tangency point and the hemisphere, and the fact that the local maximum on the conical surface for the 55-deg half-angle cone is well back toward the corner, it can be inferred that for this configuration the influence of the corner is only felt a small distance upstream. On the other hand, the heating distributions and levels for the 60 and 62-deg half-angle cones indicate that the influence of the corner is felt all the way to the stagnation point.

Distributions of shock-layer thickness, surface pressure, and sonic line locations for the hemisphere and spherically capped, conical bodies are presented in Fig. 14 for entry into the Uranus cool atmosphere. These results, together with those presented in Fig. 13, show how the character of the flow changes with large shifts in sonic line location. The shock-layer thickness is significantly greater over the entire surface when the sonic line is located in the vicinity of the corner than when it is forward near the sphere-cone tangency point. The pressure distributions for rearward sonic line location lack the overexpansion (local minimum) and decay more gradually toward the corner than for the forward sonic line location. Finally, it is seen that the flow forward of the tangency point and sonic line locations are similar to those of the hemisphere only when the sonic line is forward.

The approximation of effects of small excursions in angle of attack for entry into the Jupiter nominal model atmosphere are shown in Figs. 15 and 16. Freestream conditions are those

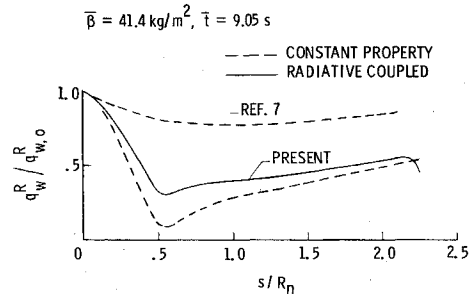

Fig. 17 Comparison of methods for Saturn entry in nominal atmosphere.

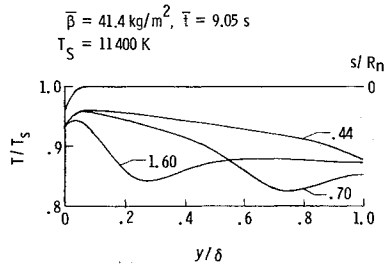

Fig. 18 Shock-layer temperature profiles for Saturn entry in nominal atmosphere.

for peak stagnation-point radiative heating ($\bar{t}$=8.09) for the heating pulse presented in Fig. 4. For all cone angles studied, the sonic line is forward and the general features of the heating distributions, shock-layer thicknesses, and pressure distributions indicate an insignificant forward influence of the corner. However, a change in cone half-angle from 55 to 62 deg, or a change in angle of attack from -5 to +2 deg, results in a change in maximum heating on the conical surface from 180 to 400 MW/m^2.

These results seem to provide a good argument for re-examining the spherically capped, 60-deg half-angle cone as a candidate configuration for outer planet entry probes. Uncertainties in gas composition, and hence normal shock density ratio, can lead to large uncertainties in radiative heating. Similarly, small excursions in angle of attack can also result in large excursions in radiative heating. Thus, it becomes particularly difficult to obtain accurate predictions of heat load and subsequent ablation mass loss. A configuration with a smaller cone angle might be less subject to large variations in flank heating due to sonic line movement and angle-of-attack excursions.

The present results are the first for which the shock shape and sonic line locations have been considered in detail in calculations of the radiative heating rates about entry probes for the outer planets. As mentioned in Sec. I, a recent study[7] of Saturn and Uranus entries had to rely on specification of the shock shape by an approximate method. The radiative heating to the body was then calculated by assuming the properties across the shock layer to be constant at local shock values. The results were referred to as cold-wall, radiative heating rates. A similar analysis, referred to as a constant property analysis, was performed in the present study for a Saturn entry condition, except the shock shape was taken from a radiative coupled solution. The constant property results are compared with the equivalent, radiative coupled solution and with the results of Ref. 7. in Fig. 17. The approximate method of Ref. 7 overpredicts the radiative heating along the body surface. The differences are attributed to a more open shock shape, hence larger shock angles, used in Ref. 7 as compared with the present calculated shock shape. Larger shock angles lead to increased shock temperatures and radiative heat fluxes.

The temperatures across the shock layer for selected body points are shown in Fig. 18 for the present, coupled solution.

The interior temperatures are greater than the shock temperature, due to the entropy layer. The minimums in the profiles at body locations of 0.7 and 1.6 correspond to the streamline that originates where the local shock angle is a minimum. The radiative transport is weakly coupled to the solution with cooling effects confined to a region near the body, $y/\delta < 0.1$. Because the temperature profiles are significantly nonuniform along the body, it is unreasonable to expect that adequate results for the radiative heating distribution about an entry probe can be determined by using approximate techniques which are based on constant shock properties or extrapolation of stagnation region results.

V. Conclusions

A study has been conducted to define the radiative heating-rate distributions about a spherically capped, 60-deg half-angle conical entry probe for the outer planets Uranus, Saturn, and Jupiter. The results are the first in which shock shapes and sonic line locations have been considered in detail for solutions of radiative heating rates at conditions that are currently under consideration for outer planet probes. These results show that both the magnitude and distribution along the body of radiative heating rate are strongly dependent on freestream conditions and the gas composition (mass fraction of hydrogen).

The radiative heating rates to the stagnation point of a body can range from values which are negligible for Uranus entries for a warm or nominal atmospheric model to the extremely high value of 1670 MW/m^2 for an entry to Jupiter for a cool atmospheric model. The radiative heating rates decrease along the forward region of the body to a minimum value at the sphere-cone tangency point and then increase along the cone flank to values, depending on freestream conditions and atmospheric model, which vary from only slightly greater than the minimum up to values 30% greater than the stagnation-point value.

It was found that the radiative heating rates on the flanks of the spherically capped, 60-deg half-angle conical body were extremely sensitive to movements of the sonic line location in the shock layer and to small excursions in angle of attack as approximated by varying cone half-angle. Thus, it would appear that this configuration should be re-examined as a candidate for an outer planet entry probe; a smaller cone half-angle should also be considered.

Shock-layer temperature profiles were found to be significantly nonuniform about the body. Because radiative heating is strongly influenced by temperature, it is doubtful that adequate results for the radiative heating rates along the body can be predicted by approximate techniques which are based on constant shock-layer properties or extrapolation of stagnation-region results.

References

[1] Sutton, K., "Characteristics of Coupled Nongray Radiating Gas Flows with Ablation Products Effects about Blunt Bodies during Planetary Entries," Ph. D. Thesis, Dept. of Mechanical and Aerospace Engineering, N.C. State Univ. at Raleigh, 1973 (available as NASA TM X-72078).

[2] Sutton, K., "Fully Coupled Nongray Radiating Gas Flows with Ablation Product Effects about Planetary Entry Bodies," *AIAA Journal,* Vol. 12, Aug. 1974, pp.1099-1105.

[3] Sutton, K., "Coupled Nongray Radiating Flow about Ablating Plantary Entry Bodies," *AIAA Journal,* Vol. 12, Aug. 1974, pp.1099-1105.

[4] Falanga, R.A. and Olstad, W.B., "An Approximate Inviscid Radiating Flowfield Analysis for Sphere-Cone Venusian Entry Vehicles," AIAA Paper 74-758, Boston, Mass., 1974.

[5] Tauber, M. E. and Wakefield, R.M., "Heating Environment and Protection during Jupiter Entry," *Journal of Spacecraft and Rockets*, Vol. 8, June 1971, pp. 630-636.

[6] Tauber, M.E., "Heat Protection for Atmospheric Entry into Saturn, Uranus, and Neptune," American Astronautical Society Preprint AAS-71-145, Washington, D.C., 1971.

[7] Nicolet, W.E., Morse, H.L., and Vojvodrich, N.S., "Outer Planet Probe Entry Thermal Protection-Part I. Aerothermodynamic Environment," AIAA Paper 74-700, Boston, Mass., 1974.

[8] Nicolet, W.E., Howe, J.T., and Mezines, S.A., "Outer Planet Probe Entry Thermal Protection-Part II. Heat-Shielding Requirements," AIAA Paper 74-701, Boston, Mass., 1974.

[9] Barnwell, R. W., "A Time-Dependent Method for Calculating Supersonic Angle-of-Attack Flow about Axisymmetric Blunt Bodies with Sharp Shoulders and Smooth Nonaxisymmetric Blunt Bodies," NASA TN D-6283, 1971.

[10] Barnwell, R.W., "Three-Dimensional Flow around Blunt Bodies with Shoulders," AIAA Paper 71-56, New York, 1971.

[11] Allen, H. J. and Eggers, A.J., Jr., "A Study of the Motion and Aerodynamic Heating of Ballistic Missiles Entering the Earth's Atmosphere at High Supersonic Speeds," NACA TR-1381, 1958.

[12] Sutton, K. and Graves, R.A., Jr., "A General Stagnation-Point Convective-Heating Equation for Arbitrary Gas Mixtures," NASA TR R-376, 1971.

[13] "The Planet Jupiter (1970)," NASA SP-8069, 1971.

[14] "The Planet Saturn (1970)," NASA SP-8091, 1971.

[15] "The Planets Uranus, Neptune, and Pluto (1971)," NASA SP-8103, 1972.

[16] Page, W.A., "Aerodynamic Heating for Probe Vehicles Entering the Outer Planets," American Astronautical Society Preprint AAS-71-144, 1971.

[17] Cooper, D.M. and Borucki, W.J., "Measurements of Hydrogen-Helium Radiation at Shock-Layer Temperatures Appropriate for Jupiter Entry," *Journal of Quantitative Spectroscopy and Radiative Transfer,* Vol.13, Oct. 1973, pp.1047-1051.